Tail Design of A Miniature Two-Wheg Climbing Robot for External Transitioning

Audelia G. Dharmawan, Darren C. Y. Koh, Gim Song Soh*, Shaohui Foong, Roland Bouffanais, and Kristin L. Wood

Singapore University of Technology and Design, Singapore,
*sohgimsong@sutd.edu.sg

Abstract. Plane-to-plane transitioning is essential for climbing robots to overcome obstacles. In existing literature, additional actuator or robot module is usually required for external transitioning, which significantly increases both size and weight of the robot. Recently, it has been shown [1] that a simple passive vertical tail can aid a lot in achieving external transitioning. This paper extends that finding and outlines a quasi-static kinematic procedure to design the tail shape for increased performance. The systematic approach is described, followed by a discussion of the results obtained. The outcome of the approach can be used to design the shape of the climbing robot's tail which enhances certain criteria for transitioning, such as the adhesive and motor torque requirements.

Keywords: climbing robot, external transition, tail design

1 Introduction

Miniature climbing robots exhibit many advantages, such as a greatly-expanded workspace and the capacity to reach or execute otherwise impossible spots or missions for ground robots. To perform the tasks, the robot may be required to climb obstacles and transit from one plane to another, both internally (concave angle between the surfaces) and externally (convex angle). Among the various attachment means, such as magnetic [2], vacuum suction [3], gripping [4], and electro-adhesive [5], dry adhesives have the benefits of being lightweight, energy efficient, and operationally quiet to be used in miniature climbing robots [6].

There are several different existing types of climbing robots which utilize dry adhesives, for example track-based [7], legged [8], and wheel-leg (wheg) [9–11]. It has been observed from nature that the mechanism for attachment to the surface in climbing animals is completely different from its detachment [12]. The general principle is found to be an entire-surface attachment and a peeling-like detachment such that strong adhesion is instantaneously generated while minimal effort is needed for contact release. For miniature robots, designing bulky legged mechanism to fulfil this motion is undesirable. While a track-based vehicle is unable to produce this locomotion, a more effective approach is to employ the wheg configuration with compliant adhesive to passively achieve the required motion.

© Springer Nature Switzerland AG 2019

T. Uhl (ed.), *Advances in Mechanism and Machine Science*,
Mechanisms and Machine Science 73,
https://doi.org/10.1007/978-3-030-20131-9_212

Wheg-based climbing robots also have outstanding ability to perform interior transitions due to the compliant feet naturally contacting the adjacent climbing surface [13]. However, external transitions have been found to be a challenge [14, 15]. Additional active tail or body joint is usually needed [13, 16, 17] to support the rear section of the climbing robot while the front part performs the external transitions. These then require extra actuators and/or body segments which increase the size and mass of the miniature robot significantly.

Design optimization is usually carried out to obtain the most advantageous robot parameters which enhance its climbing capabilities. For example, the length of the robot, which includes the length of the tail, was optimized in [18] to maximize the theoretical factor of safety for climbing. The location of the body joint was optimized in [13] to improve external transitioning. The tread thickness and the body length were optimized in [16] to enhance transitioning efficiency. The compliant body joint and the active tail were optimized in [17] to increase climbing stability.

It has been found through in-depth analysis [1] that adding a simple passive vertical tail can incredibly aid external transitions while keeping the size of the robot compact. In that paper, only the presence of the vertical tail was analyzed. The objective of this paper is to extend the finding and propose a systematic approach to further design the shape of the tail which minimizes certain requirements for performing the external transitions, such as the adhesive force and motor torque required. This can in turn increase the payload as well as the speed capability of the climbing robot.

2 The Two-Wheg Climbing Robot (Orion)

As shown in Fig. 1(a), the architecture of our climbing robot (Orion) can be categorised into three parts: whegs, chassis, and tail. The chassis houses similar electronics as the other version published previously [19], and consists of two DC motors each driving a wheg with four "flaps" equipped with a compliant dry adhesive. There is a 4:1 gear reduction between the motor and the wheg. The robot has a vertical tail component which helps in accomplishing external transitions, which distinguishes it from the previous versions [19, 20]. The robot's dimensions are 100 mm $\times$ 82 mm $\times$ 64 mm and the weight is 137.5 g.

The dry adhesive used in the climbing robot consists of three layers: a 0.8 mm AirStick^{TM} Microsuction tape by Sewell, a 0.18 mm plastic sheet, and a 3M VHB tape. The surface of a microsuction tape consists of thousands of microscopic air pockets which can create partial vacuums between the tape and the target surface. The thinness of the microsuction tape makes it very susceptible to deformation, and hence an additional flexible plastic sheet is added to help the compliant microsuction tape to return to its original flat shape to encourage maximum contact between the adhesive and surface. The unstructured backing layer of polymer (3M tape) of different elastic behaviour creates a gradient in the viscoelastic property, which has been shown to enhance the adhesive force of the dry adhesive [21].

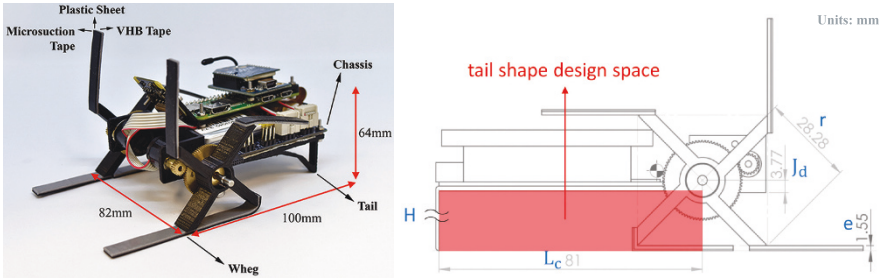

Fig. 1. (a) The miniature two-wheg climbing robot with vertical tail component for robust transitioning capabilities and (b) Geometric parameters of the robot.

Figure 1(b) shows the dimensions of the climbing robot and the full tail shape design space as a vertical tail component is added to the climbing robot for robust transitioning capability. Given the infinite possibility of the shape of the vertical tail, it is thus useful to design the optimum tail height and curve shape within the possible design space that also minimize key criteria such as the adhesive and motor torque requirements.

3 Method

In this section, the approach used to generate the shape of the robot's vertical tail component such that it minimizes the required normal adhesive force and motor torque for 4-way external transitions is described. It consists of four steps which we will illustrate each in detail.

3.1 Determination of Vertical Tail Height

The first step involves the determination of the vertical tail height (H_c) that yields the minimum required initial normal adhesive force for the 4-way external transitions (see Fig 2(a)). To determine H_c, the required initial normal adhesive forces based on the different possible vertical tail height H and the wheg first contact distance q for each transition behavior are obtained and plotted. From the data plot, the vertical tail height that yields the minimum required initial normal adhesive force among the 4-way transition are selected as H_c. Note that this analysis also takes into consideration if the chassis is in contact with the surface, loses contact with the surface or whether its vertical tail component is missing (refer to [1] for details).

3.2 Kinematic Analysis of External Transitioning

The second step involves kinematic analysis of the climbing robot to determine its joint parameters as it performs the external transition under a variety of

tail shape or contact geometry. Figure 2(a) shows the kinematic model of the robot at the start of the external transition for a chosen vertical tail height (H_c). As the climbing robot executes the external transition, other than the contact between the wheg and the surface, there is a point on the robot body that will be in contact with the surfaces' intersecting corner ($\mathbf{U}$) so that equilibrium can be maintained. Let the initial contact point be specifically denoted as point $\mathbf{U_c}$. The triangle $\mathbf{U_cV_eB_e}$ then forms the design space $\mathbf{\Omega}$ for the shape of the tail geometry connecting $\mathbf{U_c}$ to $\mathbf{B_e}$.

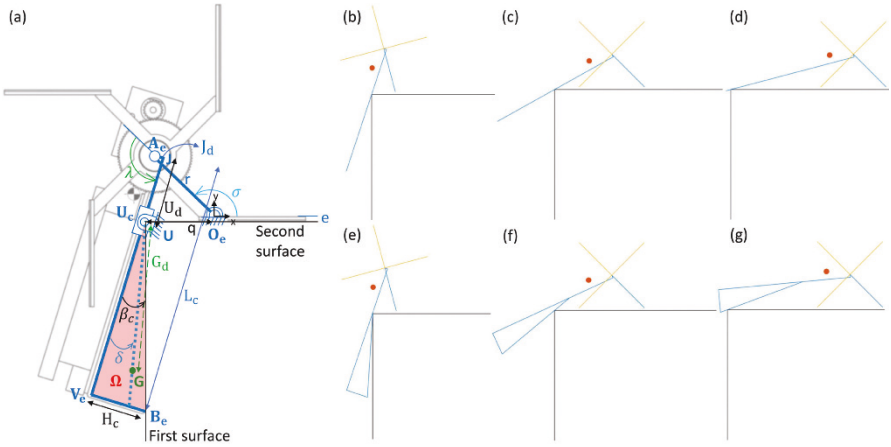

Fig. 2. (a) Kinematic model of the climbing robot's motion during external transition, (b)-(d) Simulated motion of the robot transiting externally with $\delta = 0$, (e)-(g) Simulated motion of the robot transiting externally with $0 < \delta < \beta_c$.

After the initial contact, the shape of the vertical tail determines the set of continuous contact points with $\mathbf{U}$ as the climbing robot performs the external transition. The profile made by these contact points dictates the configuration of the robot at any instance and thus affects the overall adhesive requirement. The coordinate transformation of a point $\mathbf{G}$ inside the tail design space $\mathbf{\Omega}$ relative to an origin frame at point $\mathbf{O_e}$ is given by

$$\begin{Bmatrix} \mathbf{G} \\ 1 \end{Bmatrix} = Z(\sigma)X(r)Z(\lambda + 90°)X(J_d)Z(-90°)X(U_d)Z(\delta)X(G_d)\begin{Bmatrix} 0 \\ 0 \\ 1 \end{Bmatrix}$$
$$= \begin{Bmatrix} r\cos\sigma + U_d\cos(\sigma+\lambda) - J_d\sin(\sigma+\lambda) + G_d\cos(\sigma+\lambda+\delta) \\ r\sin\sigma + U_d\sin(\sigma+\lambda) + J_d\cos(\sigma+\lambda) + G_d\sin(\sigma+\lambda+\delta) \\ 1 \end{Bmatrix} \equiv \begin{Bmatrix} q \\ e \\ 1 \end{Bmatrix} \quad (1)$$

where $Z(a)$ is a rotation of an angle a about the Z-axis, $X(l)$ is a translation of a distance l along the X-axis, σ is the angle between the adhesive and the

corresponding wheg spoke, λ is the angle between the corresponding wheg spoke and the robot's chassis, r is the wheg's radius, J_d is the distance between the wheg's shaft and the chassis, U_d is the distance along the robot's chassis between the wheg's shaft and the point $\mathbf{U_c}$, δ is the angle variable measured from the robot chassis, G_d is the distance variable measured from point $\mathbf{U_c}$, q is the distance between the pivot point on the adhesive ($\mathbf{O_e}$) and the intersecting corner ($\mathbf{U}$), and e is the adhesive's thickness.

By varying the values of δ and G_d with $\delta \in [0, \beta_c)$ and $G_d \in (0, (L_c - U_d)\sec\delta)$ where β_c is the angle between the robot's chassis and the first surface at the initial contact configuration and L_c is the length of the robot's chassis, different locations of point $\mathbf{G}$ inside the tail design space $\mathbf{\Omega}$ can be analyzed for its adhesive requirement. G_d can also be varied by rotating the wheg forward, i.e. varying the values of σ. Given the varying δ and σ, solving Eq. (1) gives the joint parameters value of λ and G_d that correspond to the instance that a certain point $\mathbf{G_i}$ inside the tail design space $\mathbf{\Omega}$ is in contact with the intersecting corner $\mathbf{U}$ (see Fig. 3(b)). It has to be noted that, if after rotating the wheg forward, the next wheg flap becomes in contact with the surface, the value of q has to be replaced with $q + (n-1)r\sqrt{2}$ where n denotes the n^{th} wheg flap to be in contact with the second surface. Figure 2(b)-(g) shows the samples of simulated motion of the robot performing the external transition for two different δ values. The blue spoke denotes the primary wheg in contact with the surface along the motion.

3.3 Adhesive Force Requirement within Tail Design Space

The third step involves the determination of the required normal adhesive force based on the robot configuration as it performs the external transition at the various contact points $\mathbf{G_i} \in \mathbf{\Omega}$. The required normal adhesive force (F_{Rne}) can be obtained from [1] depending on which case the robot's behaviour falls into. The free body diagram (see Fig. 3(a)) and the equations are restated here with slight adaptation for completeness (refer to [1] for details).

$$F_G = \frac{W}{q\sin\beta_d}(L_{ycge}\sin\theta + L_{xcge}\cos\theta) \tag{2}$$

Case I Tail is in contact with the surface ($F_G > 0$)

$$F_{Rne} = W\sin\theta - \frac{W}{q}(L_{ycge}\sin\theta + L_{xcge}\cos\theta) \tag{3}$$

Case II Tail loses contact with the surface ($F_G \leq 0$)

$$F_{Rne} = W\sin\theta \tag{4}$$

Case III Vertical tail component is absent ($\beta_c = 0$)

$$F_{Rne} = W\sin\theta \tag{5}$$

where F_G is the normal reaction force acting on the intersection between the robot's tail point $\mathbf{G_i}$ and the corner $\mathbf{U}$ in the direction perpendicular to the tail, W is the weight component of the robot acting at the robot's center of gravity (CG), θ is the slope angle of the first surface, L_{ycge} and L_{xcge} are the distances of the robot's CG from the first surface and the second surface respectively.

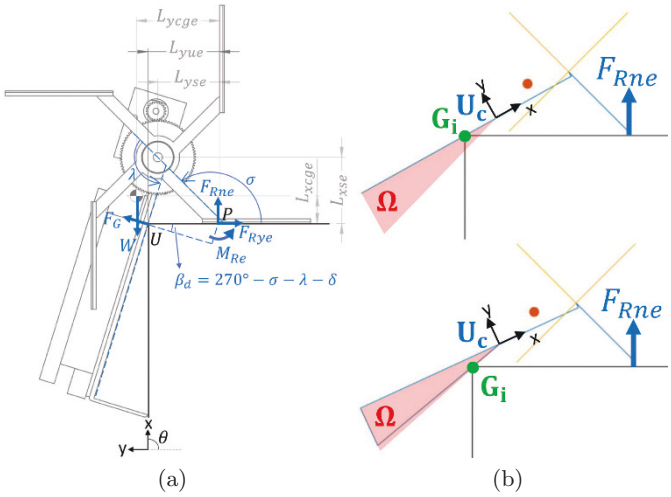

Fig. 3. (a) Free body diagram of the robot during external transition [1], (b) Different contact points $\mathbf{G_i} \in \mathbf{\Omega}$ result in different robot configuration and thus different required normal adhesive force F_{Rne}.

A contour map of the required normal adhesive force for various contact points $\mathbf{G_i}$ inside the tail design space $\mathbf{\Omega}$ can then be generated through linear interpolation. In other words, relative to a frame at point $\mathbf{U_c}$ with its x-axis directed along the robot's chassis, the value of the required normal adhesive force at a specific point ($F_{Rne}(X, Y)$) can be determined, with $(X, Y) \in \mathbf{\Omega}$. As depicted in Fig. 3(b), different possible contact points $\mathbf{G_i} \in \mathbf{\Omega}$ result in different robot configurations and thus different required normal adhesive force F_{Rne}.

3.4 Tail Shape Design

The last step is to design the curve shape of the vertical tail, based on the contour map of the required normal adhesive force obtained from the previous subsection. The $Y_{min}(X)$ position which gives the minimum absolute value of the normal adhesive force for each discretized X location is first obtained, i.e. $\min(\text{abs}(F_{Rne}(X)))$. The absolute value is minimized because, when F_{Rne} is negative, maximizing it to be nearer to zero reduces the required normal adhesive force. On the other hand, when F_{Rne} is positive, minimizing it to be nearer to zero reduces the motor torque requirement.

The above systematic procedure can then be performed for all the 4-way external transitioning by changing the value of θ in Eq. (3), (4) or (5) when calculating F_{Rne}. In other words, the $Y_{min}(X)$ locations which correspond to $\min(\text{abs}(F_{Rne}(X)))$ can be obtained for the transitioning cases of vertical up to horizontal (VU −> H), horizontal to vertical down (H −> VD), vertical down to horizontal inverted (VD −> HI), and horizontal inverted to vertical up (HI −> VU). From there, the $Y_{max,4}(X)$ locations which gives the maximum $\min(\text{abs}(F_{Rne}(X)))$ of all the four cases of external transitioning are detemined. This then gives the $Y_{max,4}(X)$ location for each discretized X location that minimizes the worst $\min(\text{abs}(F_{Rne}(X)))$ of the 4-way external transitions.

The curve shape of the tail that minimizes the normal adhesive force as well as the motor torque requirements can then be obtained by fitting a polynomial curve $P_C = P_1X^n + P_2X^{n-1} + \cdots + P_nX + P_{n+1}$ to $Y_{max,4}(X)$ with two end constraints: the curve starts at point $\mathbf{U_c}$ and ends at $\mathbf{B_e}$ to fulfil the vertical tail height (H_c) selected previously. The curve fitting problem can be written as constrained linear least-squares problem:

$$\begin{aligned} \min_{P} \quad & ||C_P(X) \cdot P - Y_{max,4}(X)||_2^2 \\ \text{such that} \quad & A_{eq} \cdot P = b_{eq} \end{aligned} \tag{6}$$

where $C_P(X) = [X^n \ X^{n-1} \ \ldots \ X \ 1]$, $P = [P_1 \ P_2 \ \ldots \ P_n \ P_{n+1}]^T$ are the coefficient terms of the fitted polynomial curve, $A_{eq} = \begin{bmatrix} C_P(L_c - U_d) \\ C_P(0) \end{bmatrix}$ and $b_{eq} = \begin{bmatrix} H_c \\ 0 \end{bmatrix}$ are the end and start constraints.

4 Results & Discussions

In this section, the results of the vertical tail design following the proposed approach described in the previous section are presented and discussed. Figure 4(a) shows the maximum normal adhesive force required as the vertical tail height is varied for the 4-way external transitions. Observed from the plot, the required normal adhesive force does not change much as the tail height is varied for the transitioning cases of H −> VD, VD −> HI, and HI −> VU. For the case of VU −> H, the required normal adhesive force reduces much up to a tail height of 15 mm. Since increasing the vertical tail height further does not affect the required normal adhesive force much while it increases the size and mass of the robot, the vertical tail height of 15 mm is selected.

Figure 4(b) shows the contour maps of the required normal adhesive force within the tail design space $\mathbf{\Omega}$ for all the 4-way external transitions. The red lines plot $Y_{min}(X)$, the Y position which gives the minimum absolute value of the normal adhesive force for each discretized X location. Figure 5(a) then shows the plot of $Y_{max,4}(X)$, the Y position which gives the maximum Y_{min} value among the four external transitions for each discretized X location. If the tail curve follows this plot, it will thus minimize the worst required normal adhesive

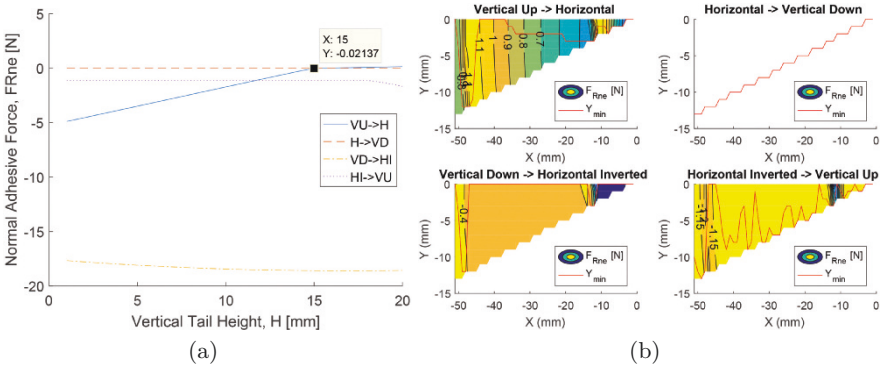

Fig. 4. (a) Plot of the normal adhesive force (F_{Rne}) for varying height of the vertical tail component for 4-way external transitions, (b) Contour maps of the normal adhesive force (F_{Rne}) within the tail design space $\boldsymbol{\Omega}$ for 4-way external transitions. The red lines plot the $Y_{min}(X)$, the Y position which gives the minimum absolute value of the normal adhesive force for each discretized X location.

force. As the data points $Y_{max,4}(X)$ is not smooth, the tail curve is designed by curve fitting using the optimization problem in Eq. (6) with a second degree polynomial. The red line plots the final shape of the tail curve with the start and end constraints satisfied.

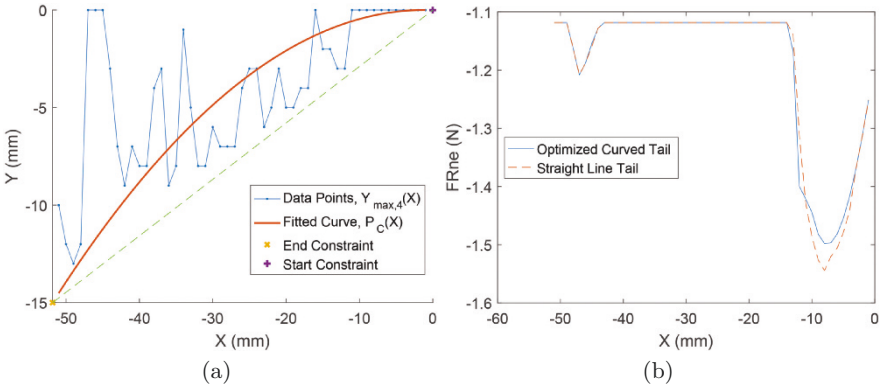

Fig. 5. (a) Plot of the synthesized tail curve, (b) Comparison between the required normal adhesive force for the synthesized curved tail and the straight line tail.

To evaluate whether the design of the tail curve shape is beneficial, Fig. 5(b) plots the value of the maximum required adhesive force as the climbing robot performs the external transitions along the X position for the synthesized

curved tail as compared to if the vertical tail is only designed as a straight line between $\mathbf{U_c}$ and $\mathbf{B_e}$ (dashed green line in Fig. 5(a)). As seen from the graph, the synthesized curved tail on average reduces the required normal adhesive force, with the maximum required adhesive force along the X position being reduced. The reduction in the required adhesive force will also result in an increase of the payload and speed of the climbing robot. Hence, designing the shape of the tail curve is beneficial in improving the performance of the robot.

5 Conclusions

In this paper, a systematic simulated procedure was proposed to design the shape of the tail of a climbing robot which minimizes certain requirements for transitioning. The motion of the robot perfoming the external transitions is modeled and simulated to obtained the robot configuration while transiting. The normal adhesive force required is then calculated along the robot's motion for different possible tail shape. Finally curve fitting is employed to synthesize the tail curve shape that minimizes the adhesive requirement. The results show that the synthesized curve shape tail helps in reducing the adhesive requirement as compared to a straight line tail. This in turn can increase the payload as well as the speed capabilities of the climbing robot. The systematic procedure can be applied to optimize other required parameters such as climbing stability etc.

6 Acknowledgements

The authors gratefully acknowledge the support of TL@SUTD - Systems Technology for Autonomous Reconnaissance & Surveillance and SUTD-MIT International Design Center (http://idc.sutd.edu.sg)

References

1. D. C. Y. Koh, A. G. Dharmawan, H. H. Hariri, G. S. Soh, S. Foong, R. Bouffanais, H. Y. Low, and K. L. Wood, "Design and Analysis of A Miniature Two-Wheg Climbing Robot with Robust Internal and External Transitioning Capabilities," in *Proc. IEEE Int. Conf. Robot. Autom.*, in press, 2019.
2. F. Tâche, W. Fischer, R. Siegwart, R. Moser, and F. Mondada, "Compact magnetic wheeled robot with high mobility for inspecting complex shaped pipe structures," in *Proc. IEEE/RSJ Int. Conf. Intell. Robots Syst.*, pp. 261-266, 2007.
3. G. Lee, H. Kim, K. Seo, J. Kim, and H. S. Kim, "MultiTrack: A multi-linked track robot with suction adhesion for climbing and transition," *Robot. Auton. Syst.*, vol. 72, pp. 207-216, 2015.
4. M. Malley, M. Rubenstein, and R. Nagpal, "Flippy: A soft, autonomous climber with simple sensing and control," in *Proc. IEEE/RSJ Int. Conf. Intell. Robots Syst.*, pp. 6533-6540, 2017.
5. H. Prahlad, R. Pelrine, S. Stanford, J. Marlow, and R. Kornbluh, "Electroadhesive robotswall climbing robots enabled by a novel, robust, and electrically controllable adhesion technology," in *Proc. IEEE Int. Conf. Robot. Autom.*, pp. 3028-3033, 2008.

6. R. Sahay, H. Y. Low, A. Baji, S. Foong, and K. L. Wood, "A State-of-the-Art Review and Analysis on the Design of Dry Adhesion Materials for Applications such as Climbing Micro-robots," *RSC Adv.*, vol. 5, no. 63, pp. 50821-50832, 2015.
7. O. Unver, and M. Sitti, "Tankbot: A miniature, peeling based climber on rough and smooth surfaces," in *Proc. IEEE Int. Conf. Robot. Autom.*, pp. 2282-2287, 2009.
8. O. Unver, and M. Sitti, "A miniature ceiling walking robot with flat tacky elastomeric footpads," in *Proc. IEEE Int. Conf. Robot. Autom.*, pp. 2276-2281, 2009.
9. K. A. Daltorio, T. E. Wei, S. N. Gorb, R. E. Ritzmann, and R. D. Quinn, "Passive foot design and contact area analysis for climbing mini-whegs," in *Proc. IEEE Int. Conf. Robot. Autom.*, pp. 1274-1279, 2007.
10. M. P. Murphy, W. Tso, M. Tanzini, and M. Sitti, "Waalbot: An agile small-scale wall climbing robot utilizing pressure sensitive adhesives," in *Proc. IEEE/RSJ Int. Conf. Intell. Robots Syst.*, pp. 3411-3416, 2006.
11. A. G. Dharmawan, P. Xavier, D. Anderson, K. B. Perez, H. H. Hariri, G. S. Soh, A. Baji, R. Bouffanais, S. Foong, H. Y. Lee, and K. L. Wood, "A Bio-Inspired Miniature Climbing Robot with Bilayer Dry Adhesives: Design, Modeling, and Experimentation," in *Proc. ASME Int. Des. Eng. Tech. Conf. Comput. Inform. Eng. Conf. (IDETC/CIE)*, pp. V05BT07A036, 2018.
12. K. A. Daltorio, A. D. Horchler, S. Gorb, R. E. Ritzmann, and R. D. Quinn, "A small wall-walking robot with compliant, adhesive feet," in *Proc. IEEE/RSJ Int. Conf. Intell. Robots Syst.*, pp. 3648-3653, 2005.
13. K. A. Daltorio, T. C. Witushynsky, G. D. Wile, L. R. Palmer, A. A. Malek, M. R. Ahmad, L. Southard, S.N. Gorb, R.E. Ritzmann, and R. D. Quinn, "A body joint improves vertical to horizontal transitions of a wall-climbing robot," in *Proc. IEEE Int. Conf. Robot. Autom.*, pp. 3046-3051, 2008.
14. M. P. Murphy, and M. Sitti, "Waalbot: An agile small-scale wall-climbing robot utilizing dry elastomer adhesives," *IEEE/ASME Trans. Mechatronics*, vol. 12, no. 3, pp. 330-338, 2007.
15. W. A. Breckwoldt, K. A. Daltorio, L. Heepe, A. D. Horchler, S. N. Gorb, and R. D. Quinn, "Walking inverted on ceilings with wheel-legs and micro-structured adhesives," in *Proc. IEEE/RSJ Int. Conf. Intell. Robots Syst.*, pp. 3308-3313, 2015.
16. O. Unver, and M. Sitti, "Tankbot: A palm-size, tank-like climbing robot using soft elastomer adhesive treads," *Int. J. Robot. Res.*, vol. 29, no. 14, pp. 1761-1777, 2010.
17. T. Seo, and M. Sitti, "Tank-like module-based climbing robot using passive compliant joints," *IEEE/ASME Trans. Mechatronics*, vol. 18, no. 1, pp. 397-408, 2013.
18. M. P. Murphy, C. Kute, Y. Meng, and M. Sitti, "Waalbot II: Adhesion recovery and improved performance of a climbing robot using fibrillar adhesives," *Int. J. Robot. Res.*, vol. 30, no. 1, pp. 118-133, 2011.
19. H. H. Hariri, D. C. Y. Koh, H. C. Lim, A. G. Dharmawan, V. D. Nguyen, G. S. Soh, S. Foong, R. Bouffanais, H. Y. Low, and K. L. Wood, "ORION-II: A Miniature Climbing Robot with Bilayer Compliant Tape for Autonomous Intelligent Surveillance and Reconnaissance," in *Proc. IEEE 15th Int. Conf. Control Autom. Robot. Vis. (ICARCV)*, pp. 1621-1626, 2018.
20. A. G. Dharmawan, P. Xavier, H. H. Hariri, G. S. Soh, A. Baji, R. Bouffanais, S. Foong, H. Y. Lee, and K. L. Wood, "Design, Modeling and Experimentation of a Bio-Inspired Miniature Climbing Robot with Bilayer Dry Adhesives," *J. Mech. Robot*, vol. 11, no. 2, pp. 020902, 2019.
21. H. Shahsavan, and B. Zhao, "Bioinspired functionally graded adhesive materials: synergetic interplay of top viscouselastic layers with base micropillars," *Macromolecules*, vol. 47, no. 1, 353-364, 2013.